Real-time sonoelastography of hepatic thermal lesions in a swine model

Man Zhang[a)]
Department of Biomedical Engineering, University of Rochester, Rochester, New York 14627

Benjamin Castaneda
Department of Electrical and Computer Engineering, University of Rochester, Rochester, New York 14627

Jared Christensen, Wael Saad, and Kevin Bylund
Department of Imaging Sciences, University of Rochester Medical Center, Rochester, New York 14627

Kenneth Hoyt
Department of Electrical and Computer Engineering, University of Rochester, Rochester, New York 14627

John G. Strang and Deborah J. Rubens
Department of Imaging Sciences, University of Rochester, Rochester, New York 14627

Kevin J. Parker
Department of Biomedical Engineering, University of Rochester, Rochester, New York 14627
and Department of Electrical and Computer Engineering, University of Rochester,
Rochester, New York 14627

Sonoelastography has been developed as an ultrasound-based elasticity imaging technique. In this technique, external vibration is induced into the target tissue. In general, tissue stiffness is inversely proportional to the amplitude of tissue vibration. Imaging tissue vibration will provide the elasticity distribution in the target region. This study investigated the feasibility of using real-time sonoelastography to detect and estimate the volume of thermal lesions in porcine livers *in vivo*. A total of 32 thermal lesions with volumes ranging from 0.2 to 5.3 cm^3 were created using radiofrequency ablation (RFA) or high-intensity focused ultrasound (HIFU) technique. Lesions were imaged using sonoelastography and coregistered B-mode ultrasound. Volumes were reconstructed from a sequence of two-dimensional scans. The comparison of sonoelastographic measurements and pathology findings showed good correlation with respect to the area of the lesions ($r^2 = 0.8823$ for RFA lesions, $r^2 = 0.9543$ for HIFU lesions). In addition, good correspondence was found between three-dimensional sonoelastography and gross pathology (3.6% underestimate), demonstrating the feasibility of sonoelastography for volume estimation of thermal lesions. These results support that sonoelastography outperforms conventional B-mode ultrasound and could potentially be used for assessment of thermal therapies. © *2008 American Association of Physicists in Medicine*.
[DOI: 10.1118/1.2968939]

Key words: sonoelastography, radiofrequency ablation, high-intensity focused ultrasound, coagulation necrosis, thermal lesion, liver, swine model

I. INTRODUCTION

Thermal ablation techniques, such as radiofrequency ablation (RFA) and high-intensity focused ultrasound (HIFU), are continuously growing for the treatment of unresectable tumors in clinical practice. The main objective of thermal ablation is to induce *in situ* coagulation necrosis for complete destruction of targeted tumors, with minimal damage to the surrounding normal tissues.

In RFA, a shielded needle electrode is inserted directly to the tumor under image guidance. Radio frequency (RF) alternating current is delivered to the target tissue via the non-insulated electrode tip, causing local ion agitation that generates heat by means of friction. The heat further expands to form a necrotic lesion around the tip. Multiprong, retractable electrodes or internally cooled, straight needles are used to achieve predictable coagulation volumes. Recent studies[1] showed that RFA, as a minimally invasive technique, is capable of creating well-controlled thermal injury with fewer treatment sessions, and the procedure itself is well tolerated.

HIFU refers to a technique wherein ultrasound beams are emitted from a high-powered transducer that can target a tissue volume deep within the body. The energy deposition causes a sharp temperature increase within the focal volume, resulting in tissue coagulation necrosis and elevation of localized tissue stiffness. HIFU is currently receiving much attention due to its potential for noninvasive tumor destruction within a well-defined position. Two principal mechanisms, tissue heating and acoustic cavitation, are responsible for HIFU-induced tissue necrosis. HIFU systems commonly operate in a frequency range of 1–5 MHz, generating focal intensities of approximately 1000–10 000 W/cm^2. Such high intensities can cause irreversible cell destruction and protein denaturation in seconds.

Imaging modalities for monitoring and evaluation of the treatment process play an important role in the success of an ablation therapy. Transabdominal sonography is generally used for imaging guidance during the ablation procedure. It offers convenient real-time guidance of RFA needle placement, and is cost effective. However, high positive recurrence rates have been reported for the treatment guided by conventional sonography, which may be due to low intrinsic contrast between treated and untreated tissues and artifacts from gas bubbles formation during the heating process.[2,3] Gas bubbles appear as a hyperechoic region in sonograms. This region, however, does not accurately represent the extent of ablation. Bubbles also resolve gradually, resulting in underestimate of the lesion size. Contrast enhanced ultrasound, developed to differentiate perfused and nonperfused tissues, may provide an approach to detect tumor residuals.[4–6]

The high resolution afforded by magnetic resonance imaging (MRI) enables accurate imaging of ablated tissues. Particularly, necrotic lesions can be visualized on contrast enhanced T1- and T2-weighted images. MRI parameters have an intrinsic sensitivity to temperature change, providing near real-time thermometry. Consequently, tissue damage caused by the ablation therapy can be assessed immediately using MRI.[7] MRI offers better tissue discrimination and image quality, but is expensive, time consuming, and patient selective. Additionally, MRI compatible RFA equipment is required for visualization of the lesion.

Computed tomography (CT) is also used to predict the size of a coagulated region in the soft tissue. Unenhanced CT is normally performed for targeting and monitoring while contrast enhanced CT is applied after ablation for treatment evaluation. A better correlation of lesion size was reported between CT and pathology in comparison to conventional ultrasound.[8] In that study, thermal lesions consistently showed as a hypoattenuating region on CT images, but had variable appearance on sonograms due to the diversity of lesion echogenicity. CT imaging, however, has some disadvantages including the ionizing radiation exposure, side effects of CT contrast agents, and the extended procedure time.

Thermal ablated lesions have elevated stiffness, suggesting the use of imaging techniques to portray tissue elasticity for the evaluation of tissue ablation procedures. Over the past 2 decades, elasticity imaging modalities have been developed to image stiff lesions in soft tissues based on their elasticity contrast. They fall into two categories: ultrasound-based approaches such as vibration sonoelastography,[9–12] compression elastography,[13–15] transient elastography,[16–18] and acoustic radiation force (ARF)-related imaging[19–24] and MRI-based elastography.[25–29] In particular, Varghese *et al.*[30,31] illustrated the feasibility of *in vivo* compression elastography in monitoring or imaging the stiffness of RFA lesions. Close correspondence was observed between elastographic image features and gross pathology. *In vivo* ARF impulse (ARFI) imaging was investigated by Fahey *et al.*[32,33] for monitoring RF ablation of cardiac and liver tissues, and qualitative comparisons of lesion shape, size, and relative location were found to be feasible between ARFI imaging

and pathology. However, only a few reports on *in vivo* elasticity imaging of HIFU lesions are available in the literature. Souchon *et al.*[34] presented the preliminary results of elastographic guidance of HIFU therapy in human prostate. Further study[35] compared the elastography to the MRI for the measurement of HIFU lesions, and confirmed the potential of elastography for imaging HIFU lesions in the prostate.

In sonoelastography, external vibration (amplitude < 50 μm, frequency < 1 kHz) is induced into the target tissue. The resulting tissue motion is then imaged with ultrasound pulse-echo technique specifically modified to detect vibration via real-time Doppler technique.[11,36,37] Generally, tissue stiffness is inversely proportional to the amplitude of internal vibration. Our previous *in vitro* study[38] indicated that sonoelastography improved visualization of the boundaries of RFA lesions when compared to B-mode ultrasound. Hence, the availability of sonoelastography may prospectively add more clinical information to traditional sonography and lower the costs of thermal therapies.

In this study, real-time sonoelastography was utilized to image hepatic thermal lesions in a swine model. Many of the difficulties for imaging human, including the respiratory and cardiac motion artifacts, are also present in this model. It would be essential to induce uniform and strong vibrations into the liver for *in vivo* sonoelastography. Accordingly, the purpose of this work was to investigate the feasibility of real-time sonoelastography for the detection of hepatic thermal lesions under *in vivo* conditions. Lesions of various sizes were induced in the porcine liver using RFA and HIFU techniques. The dimensions, areas, and volumes of these lesions were measured from sonoelastograms and compared to gross pathology results. The detectability and accuracy of sonoelastography were compared to those of B-mode ultrasound.

II. MATERIALS AND METHODS

Three to five thermal lesions were created and imaged on each of nine pigs using an open abdomen approach, which is detailed in Secs. II A–II C. Transcutaneous procedures were then performed on two additional pigs. This approach is described in Sec. II D.

II.A. Animal preparation

Nine pigs (weight 100 ± 10 lbs) were used in open abdomen study. Anesthesia was induced by an ear vein intubation with a mixture of ketamine ($22-33$ mg/kg), acepromazine (1.1 mg/kg), and atropine (0.05 mg/kg). The anesthetized animal was placed in dorsal recumbency on a warming blanket to maintain its body temperature. Subsequently, the abdomen was shaved for laparotomy which was performed along the ventral midline and paracostal area to expose the liver. The hair on the back was also shaved for grounding pads used for RF ablation. These procedures were performed by the professionals at the Division of Laboratory Animal Medicine following the animal use protocol approved by the University Committee on Animal Resources at the University of Rochester.
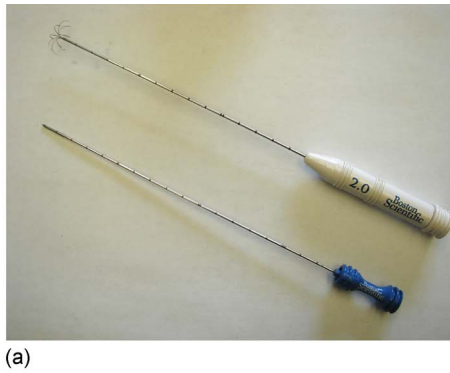
(a)
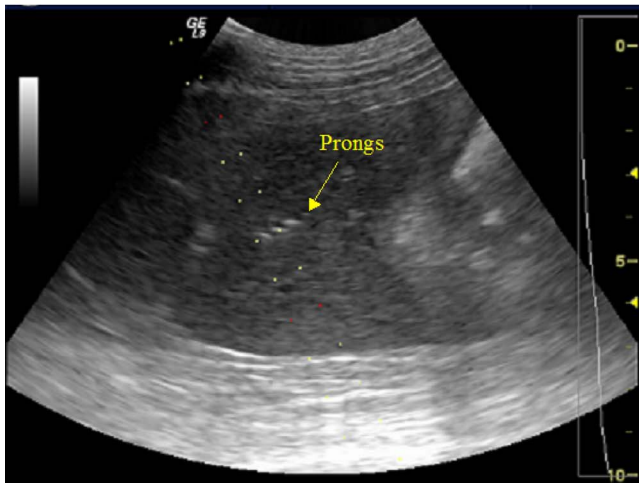
(b)

FIG. 1. LeVeen™ and Soloist™ electrodes used in the RFA procedure (a). Note that the LeVeen™ needle has eight retractable prongs that are deployed to form umbrella shape with radial diameter of 2 cm. RFA needle insertion was guided by B-mode ultrasound (b). Deployed needle prongs present as three hyperechoic short lines in the middle of this image.

II.B. Thermal lesion creation

Two types of thermal lesions, either applying RFA or HIFU techniques, were generated in porcine livers. To create a RFA lesion, four grounding pads were attached to the back of the animal followed by a needle electrode insertion under the guidance of B-mode ultrasound. A LeVeen™ needle (Boston Scientific, Natick, MA) with 2 cm diameter tip prongs or a straight Soloist™ needle (Boston Scientific, Natick, MA) was used to obtain lesions of different sizes [Fig. 1(a)]. The grounding pads and electrode were connected to a RF generator (RF 3000 Radiofrequency Ablation System, Boston Scientific, Natick, MA). When the tip of the LeVeen™ needle reached the target region, the umbrella-shaped prongs were deployed. A current from the RF generator passed through the prongs to the liver tissue, and returned through the grounding pads. Following an established protocol,[39] a RFA lesion was created $1-2$ cm beneath the liver surface in approximately 5 min. Figure 1(b) illustrates a sonogram of the inserted RFA needle, in which the deployed prongs are clearly seen. After RF ablation, the prongs were undeployed and the needle was pulled out.

Figure 2 shows a concave transducer that generates HIFU

(a)
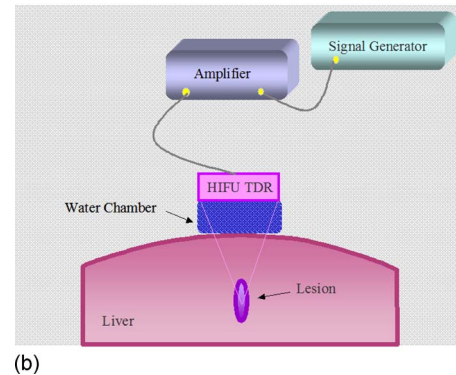
(b)

FIG. 2. The single-element concave transducer (a) used to generate HIFU beams in the experiment and the schematic diagram of the *in vivo* HIFU experimental setup (b).

beams, and a schematic diagram of the *in vivo* HIFU experimental setup. This system includes a signal generator, a RF amplifier, the HIFU transducer, and a small chamber filled with degassed water. The HIFU source is a single-element focused transducer with a focal length of 6 cm and a diameter of 5 cm (Sonic Concepts, Inc., Bothell, WA). The focal intensity of the HIFU transducer is about 1000 W/cm². A continuous sinusoidal signal (frequency: 1.1 MHz, voltage: 0.95 V) produced by a function generator passed through the amplifier and drove the transducer to generate HIFU beams. The position of the HIFU transducer was adjusted to 4 cm above the liver surface. The water chamber was used as the acoustic coupling between the transducer and the liver surface. The bottom of the water chamber was made of an acoustic-transparent film and adjusted to barely touch the liver surface. Prior to this animal study, *in vitro* experiments were conducted using the abovementioned setup, in which HIFU lesions were created after a minimum of 5-s HIFU application in the bovine liver. Considering the *in vivo* conditions such as the blood perfusion and body motions, we made various-sized lesions in the porcine liver by adjusting the duration of the HIFU application between 8 and 20 s.

II.C. Imaging of thermal lesions

Sonoelastography and B-mode imaging were investigated for detecting the necrotic lesion immediately following each thermal ablation. A schematic diagram of the setup for sonoelastographic imaging is illustrated in Fig. 3. Two amplifiers (model 2706, Brüel & Kjaer, Naerum, Denmark) driven by a
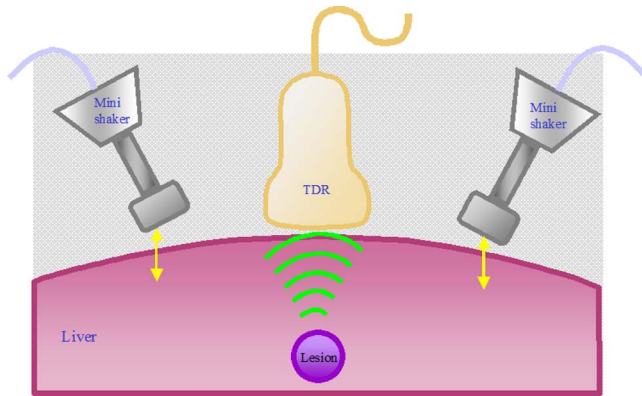
FIG. 3. Schematic diagram of the setup for sonoelastography with two external vibration sources.

harmonic waveform generator (Model 3511A Pragmatic Instruments, San Diego, CA, USA) provided input signals to two minishakers (Brüel & Kjaer, Naerum, Denmark). The minishakers, vibrating at a combination of low frequencies (105, 140, 175, and 210 Hz), were applied on the liver surface to generate a relatively uniform vibration field with displacement amplitude of approximately 20 μm for sonoelastographic imaging. The multitone vibration has been reported to effectively reduce modal artifacts in a phantom study.[40] A GE Logiq 9 ultrasound system (GE Ultrasound, Milwaukee, WI) was specifically modified to perform sonoelastographic imaging. The Doppler spectral variance of the vibrating tissue was displayed in real-time in color mode. It has been shown that the standard deviation of the power spectrum is proportional to the vibration amplitude of the tissue.[41] Coregistered sonoelastographic and B-mode images were acquired using a linear array transducer (12 MHz, GE Ultrasound, Milwaukee, WI) on the Logiq 9 scanner. The position and orientation of the imaging transducer over the liver was marked as the reference for pathology dissection. On the sonoelastograms, a stiff lesion has lower vibration amplitude and presents a black void while surrounding tissue appears bright green. By observing the location of the dark pixels, one can identify the thermal lesion (Fig. 4). A sonoelastography volume can be generated by acquiring a series of two-dimensional (2D) scans with the imaging transducer mounted on a motorized linear track (Velmex, Inc., Bloomfield, NY). The speed of the track movement was synchronized to the frame rate of the ultrasound scanner so that the interval of image acquisition was fixed to 1 mm. The sequences of sonoelastographic images and corresponding B-mode images were acquired simultaneously and saved as a cine-loop. To limit motion artifacts, the images acquired at the same phase in the respiratory cycle were used for the measurement of lesions.

After *in vivo* imaging, the animal was euthanized by an intravenous injection of 100 mg/kg of sodium pentobarbital into the ear vein. The liver was resected. For each lesion, gross pathology was obtained approximately at the same position and orientation in which it was imaged. Subsequently, gross pathology was photographed with a millimeter scale
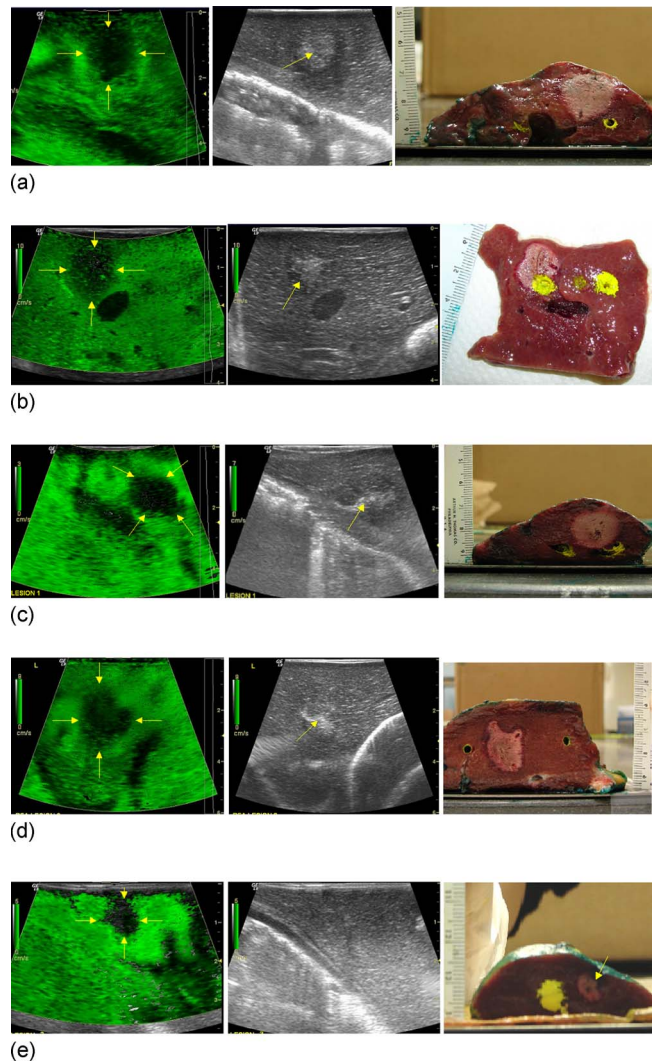
FIG. 4. Typical *in vivo* sonoelastograms, co-registered sonograms, and gross pathology photographs of RFA lesions. The bright dots on pathology photographs are markers used for later 3D reconstruction. Note that liver boundaries induce artifacts on sonoelatograms (c) and (d). The boundaries are illustrated as hyperechoic region on the coregistered sonograms. A RFA lesions as small as 0.2 cm^3 is successfully detected (e).

and considered to be ground truth. For volume estimation, thermal lesions underwent fluid displacement measurement. In this method, the dissected lesion tissue was placed into a water-filled vessel and the displacement indicated the volume of the lesion.

The average Young's moduli and elastic contrast of the thermal lesion and untreated liver tissue were obtained by mechanical testing and viscoelastic tissue modeling. Two cylindrical core samples (approximately 9 mm in diameter and 7 mm in length) were harvested from each of the three types of liver tissues (RFA lesions, HIFU lesions, and normal tissue) immediately after liver excision. Within the next 2 h, mechanical testing using a uniaxial unconfined compression was performed to measure the time-domain stress relaxation of the samples at room temperature. The resulting data was present as a plot of the stress versus time at a 5% strain. At least three repeated measurements were performed on each

of the six cores. The stress-relaxation curves were fit to the Kelvin–Voigt fractional derivative model, and the complex Young's modulus of each type of tissue was predicted and averaged in a frequency range of 100–200 Hz. Detailed description of the method can be found in our earlier articles.[42,43]

II.D. Percutaneous lesion creation and transcutaneous imaging

Percutaneous RF ablation followed by transcutaneous imaging was performed on two additional porcine livers to investigate the potential of using sonoelastography transabdominally for delineating thermal lesions. Procedures were similar to those of the open abdomen experiments, except that the lesions were created and imaged without the exposure of the liver. The vibration sources were placed on the abdomen, just touching the skin. Their positions were carefully adjusted to make a relatively strong and uniform vibration field in the liver. A 3.5 MHz curvilinear probe (GE Ultrasound, Milwaukee, WI) was used for imaging. Subsequently, the animal was euthanized and the liver was excised. The procedures for measuring the lesions were identical to those mentioned above. A total of five RFA lesions were created percutaneously, among which 3 were randomly chosen for sonoelastographic imaging.

III. RESULTS

III.A. Open abdomen approach

Typical *in vivo* sonoelastograms, coregistered sonograms, and gross pathology photographs of the RFA lesions and the HIFU lesions are shown in Figs. 4 and 5. Thermal lesions were easily visualized as dark deficits on sonoelastograms. In most of the cases, the corresponding B-mode images depicted a hyperechoic area due to the formation of gas bubbles. However, the hyperechoic area did not match the area of the lesion from gross pathology.

Thermal lesions were manually delineated by two independent observers on the 2D sonoelastograms, B-mode ultrasound images and corresponding pathology photographs (Fig. 6). Both observers had previous experience[44] with outlining stiff masses in 2D sonoelastograms and gland contours in B-mode images. First, the observers were given all gross pathology photographs in a random order to measure the lesion size from these images. Both the inner pale zone and the outer red rim of the lesion were included in the contour. Subsequently, the observers were given the 2D sonoelastograms and instructed to outline a dark deficit surrounded by a green area. When the boundary of the deficit was diffused or not completely defined, the observer completed the task by preserving a smooth shape which is expected from a thermal ablated lesion. Finally, the observers were given the B-mode images and instructed to delineate the hyperechoic regions. The observers had knowledge of the approximate position of the lesion in both B-mode and sonoelastographic images. In all cases, the area and dimensions of the lesions were estimated with NIH ImageJ software. Paired *t* tests re-

(a)

(b)

(c)

(d)
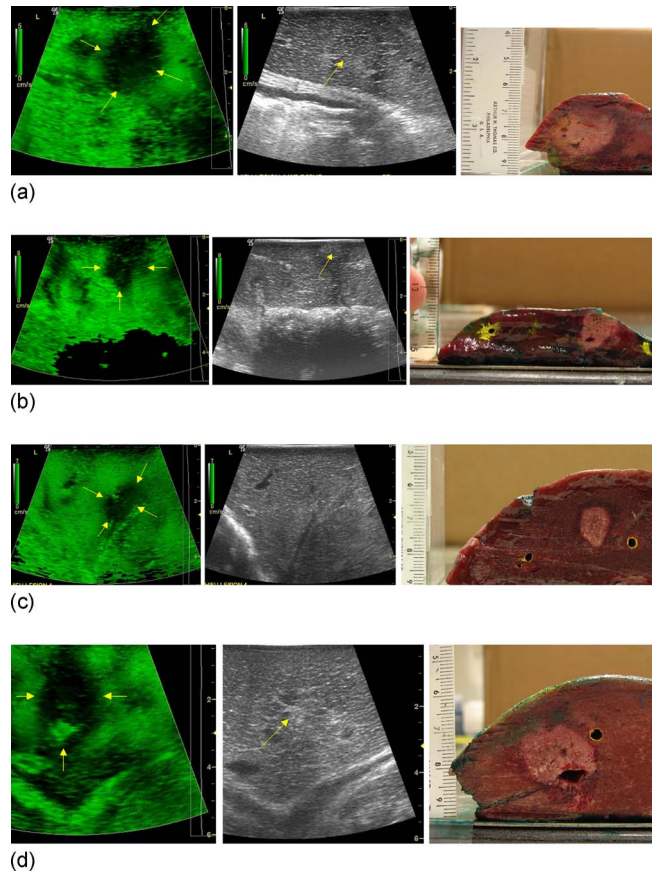
FIG. 5. *In vivo* sonoelastograms, coregistered sonograms, and gross pathology photographs of HIFU lesions. Some of the HIFU lesions are isoechoic on B-mode images but detectable on sonoelastographic images (c). If blood vessels in the lesion are not completed destructed by the HIFU approach, sonoelastography can locate them since sonoelastography is a modified Doppler technique (d).

vealed that there was no statistically significant difference between the measurements of the two observers ($p > 0.1$).

We noted that liver boundaries induced artifacts on sonoelastograms which were illustrated as hyperechoic regions on

(a)

(b)
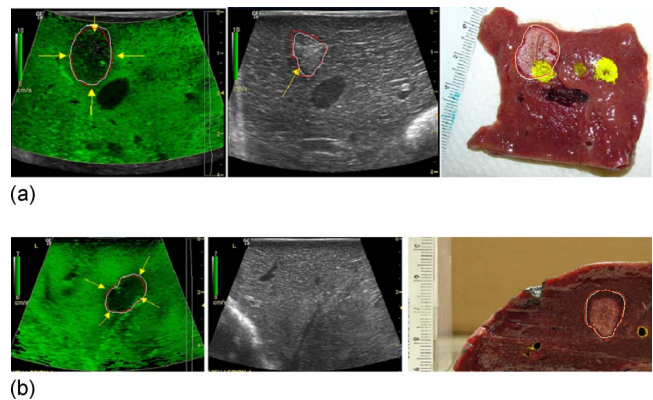
FIG. 6. Boundary delineation of the RFA lesion (a) and the HIFU lesion (b) by two independent observers on the sonoelastograms, B-mode ultrasound images, and corresponding pathology photographs. The difference between the measurements from the two observers is statistically insignificant ($p > 0.1$).

TABLE I. Boundary detection of thermal lesions using B-mode ultrasound and sonoelastography.

Boundary detection	B-mode	Sonelastography
Complete	12 (37.5%)	32 (100%)
Partial	11 (34.4%)	—
Not visualized	9 (28.1%)	—

the coregistered sonograms. In Fig. 4(b), a RFA lesion is found at the top left of the sonoelastogram next to a vessel. The gross pathology photograph confirmed the presence of the lesion next to a vessel which had collapsed after the excision of the liver. In particular, a RFA lesion as small as 0.2 cm^3 in volume, was successfully detected by *in vivo* sonoelastography [Fig. 4(e)]. Some of the HIFU lesions appeared isoechoic on B-mode images but were detectable on sonoelastograms [Fig. 5(c)]. If blood vessels in the ablated region were not fully destroyed by HIFU, an indicator of possible incomplete ablation, sonoelastography was able to locate them on the basis of the Doppler technique [Fig. 5(d)].

A total of 18 RFA lesions and 14 HIFU lesions were created in nine porcine livers, with volumes ranging from 0.2 to 4.5 cm^3 and 0.6 to 5.3 cm^3, respectively. The boundaries of all 18 RFA lesions were visualized by sonoelastography (100%) while only 6 (33.3%) were completely detected by B-mode ultrasound. For the remaining lesions, 9 were partially circumscribed (50%) and 3 were not visualized (16.7%) on B-mode. Correspondingly, all 14 HIFU lesions were completely visualized by sonoelastography (100%) but only 6 were completely detected by B-mode ultrasound (42.9%). Two of the remaining were partially contoured (14.2%), and 6 (42.9%) were missing. This result indicates that it is not reliable to use conventional ultrasound imaging for the detection of HIFU lesions. Table I compares the detectability of thermal lesion boundary between sonoelastography and B-mode ultrasound.

The scatter plot in Fig. 7 represents the association of the area measurements of the RFA lesions between pathology
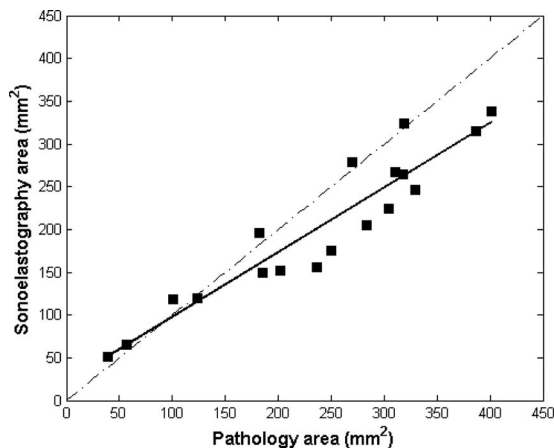
FIG. 7. Scatter plot of the area of RFA lesions at center plans between pathology and sonoelastography. A linear best fit was performed, giving a correlation (r^2) of 0.8823.
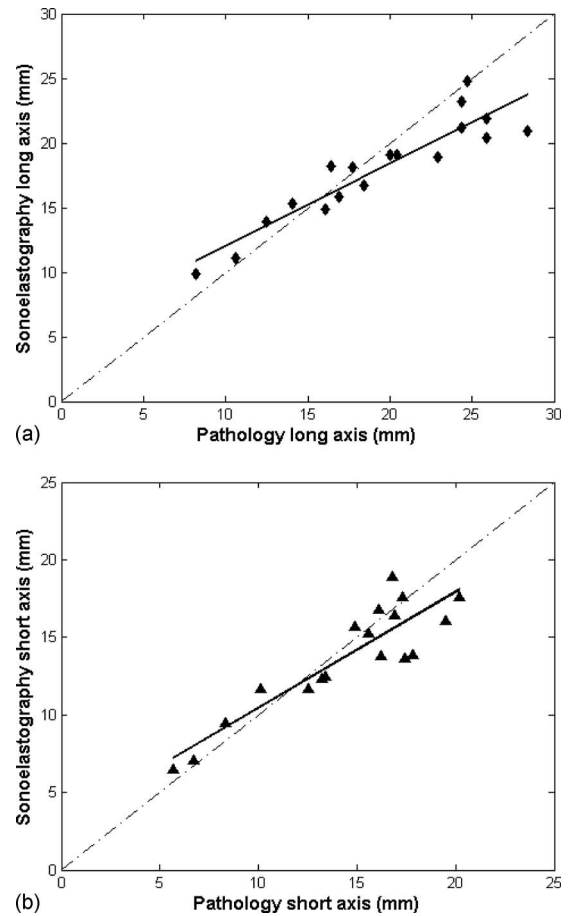
FIG. 8. Scatter plots of the long axis ($r^2=0.8534$) (a) and the short axis ($r^2=0.8098$) (b) of RFA lesions between pathology and sonoelastography.

and sonoelastography. The linear best fit was performed on this data set, giving a correlation (r^2) of 0.8823. For lesions completely visualized by B-mode, sonoelastography underestimated the lesion size by 9.9%, as opposed to 54.2% with B-mode. The principal axes of each lesion on the sonoelastogram were also measured and compared to those of pathology specimen. Again, a close correspondence was found in lesion dimensions. Scatter plots (Fig. 8) illustrate the correlation coefficients (r^2) of 0.8534 for long axis and 0.8098 for short axis, respectively.

Compared to RFA lesions, HIFU lesions are more irregular in shape. However, we found better correlations ($r^2=0.9543$ for lesion area, $r^2=0.8555$ for long axis, and $r^2=0.9079$ for short axis) for HIFU lesion areas and dimensions between sonoelastographic estimates and pathology findings (Figs. 9 and 10). On average, sonoelastography slightly underestimated the HIFU lesion area by 2.9%.

Three-dimensional (3D) reconstruction of thermal lesions allows estimation of lesion volumes. Figure 11(a) illustrates the 3D sonoelastogram of a thermal lesion generated from the parallel 2D image sequence with an interval of 1 mm. Lesion volumes were calculated from the sum of the areas in 2D images multiplied by the 1 mm separation of two adjacent images. A series of pathological cross sections of the same lesion are presented in Fig. 11(c), from which a 3D
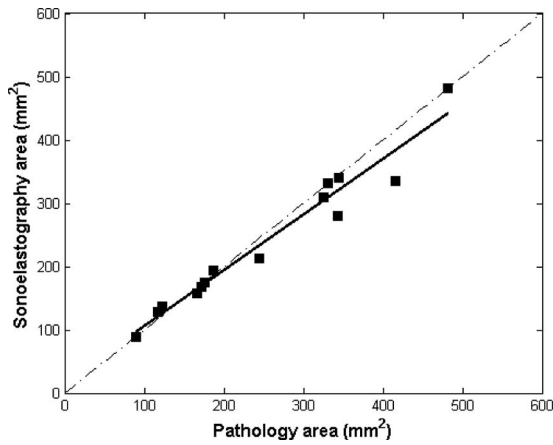
FIG. 9. Scatter plot of the area of HIFU lesions between pathology and sonoelastography ($r^2 = 0.9543$).

FIG. 11. Volume reconstruction of a RFA lesion from 2D sonoelastography images (a) and pathology photographs (b). The pathology slices of the lesion are shown in (c).

visualization of the lesion was generated [Fig. 11(b)]. In gross pathology, thermal lesions were pale in color and encircled by a red rim 2–3 mm in thickness, easily distinguishable from the untreated surrounding tissue.

Table II compares the sonoelastography volumes of six thermal lesions to their pathology volumes. Similar to the estimates of lesion areas, a consistent underestimate (3.6%)

of the volumes was found in sonoelastography. Results in Table II also demonstrate a good correspondence of the lesion volume between 3D sonoelastography and gross pathology. Tissue mechanical measurements revealed that average contrast ratios of the Young's modulus were 19:1 between RFA lesions and untreated liver tissues and 15:1 between HIFU lesions and normal liver tissues, respectively. The Young's moduli of RFA lesions, HIFU lesions, and untreated tissues were 187 ± 32 kPa, 143 ± 34 kPa, and 10 ± 3 kPa at vibration frequencies (100–200 Hz), respectively. These results are consistent with the data reported by our earlier study[42] and other groups.[45–47]

III.B. Transcutaneous approach

Transcutaneous sonoelastography depicted two RFA lesions, and the third lesion was not clearly shown on sonoelastograms. We had some difficulties in generating RFA lesions percutaneously within a single lobe of the porcine liver under the guidance of B-mode ultrasound. The accessible portion of the lobes was thin (~2 cm). In addition, the boundaries of the lobes were barely distinguishable in sonograms [Fig. 12(a)]. Consequently, two of the three investigated lesions were generated in two neighboring lobes. Moreover, the transcutaneous sonoelastography had decreased accuracy and repeatability for thermal lesion detection when compared to the open abdomen experiments. These sonoelastograms had lower signal to noise ratio due to the difficulties in coupling of the vibration sources. Over all, the results of transcutaneous sonoelastography were closely associated with pathological findings (Fig. 12).

IV. DISCUSSION

In this *in vivo* study, sonoelastography was used for visualization of necrotic lesions in the porcine liver by imaging the relative elastic contrast between lesions and normal surrounding tissue. This technique images the peak displacement of a local particle by analyzing the Doppler variance from the ultrasound echoes. Vibration fields are mapped to the ultrasound scanner screen in real-time. Good agreement of the area and volume of the RFA and HIFU lesions was found between sonoelastographic measurements and gross pathology. Sonoelastography also showed improved delectability of thermal lesions in the porcine liver when compared
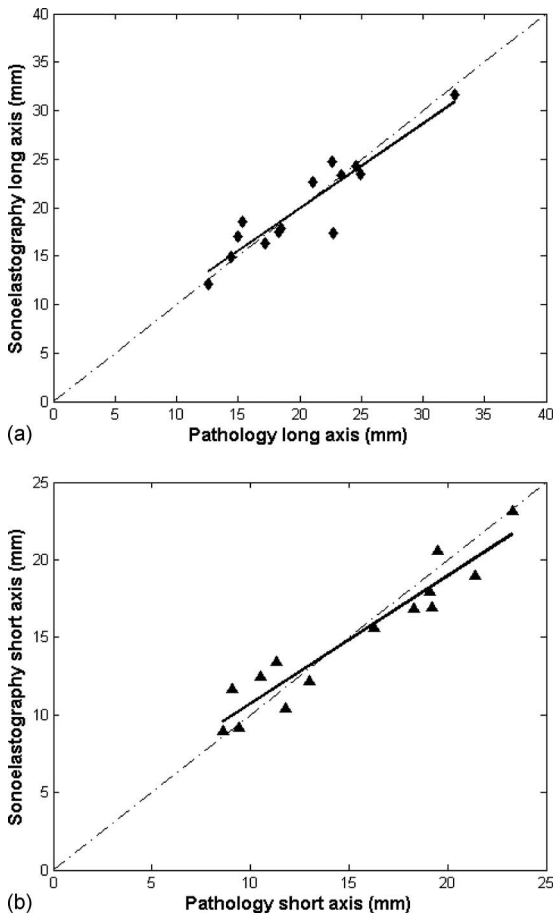
FIG. 10. Scatter plots of the long axis ($r^2 = 0.8555$) (a) and the short axis ($r^2 = 0.9079$) (b) of HIFU lesions between sonoelastography and pathology.

TABLE II. Comparison of sonoelastography volumes and pathological volumes of six thermal lesions.

	Lesion 1	Lesion 2	Lesion 3	Lesion 4	Lesion 5	Lesion 6
Path. vol. (cm^3)	2.3	3.2	3	3.5	5.7	0.6
Sonoelast. vol. (cm^3)	2	2.8	2.9	3.6	5	0.7
Difference (%)	−13.0	−12.5	−3.3	2.9	−12.3	16.7

to conventional sonography. Therefore, sonoelastography may be used to image thermal lesions and provide quantitative estimates of their size and volume. Since detection of lesion boundary is essential for decision making, sonoelastography may help clinicians evaluate therapeutic outcome immediately after treatment and during the follow-up. In addition, the results of transcutaneous sonoelastography suggested the potential of sonoelastography for non-surgical clinical implementation.

In the literature, Pareek *et al.*[48] investigated the reliability of elastography for RFA lesion detection based on an *in vivo* porcine kidney study. Statistically significant correlations were reported between elastography and pathology with respect to the area ($r = 0.9302$) and volume ($r = 0.953$) of the RFA lesion. Our correlation results are comparable with this data. Sonoelastography slightly underestimates the lesion size, which is also consistent with their findings. In the study of elastographic guidance of HIFU therapy in human prostate,[34] compression elastography visualized the HIFU lesions as low strain areas in two patients, a finding confirmed by post therapy MRI. The other 29 patients underwent whole prostate treatment. They found that those HIFU treated prostates appeared stiffer on elastograms with 40%–60% strain decreases.
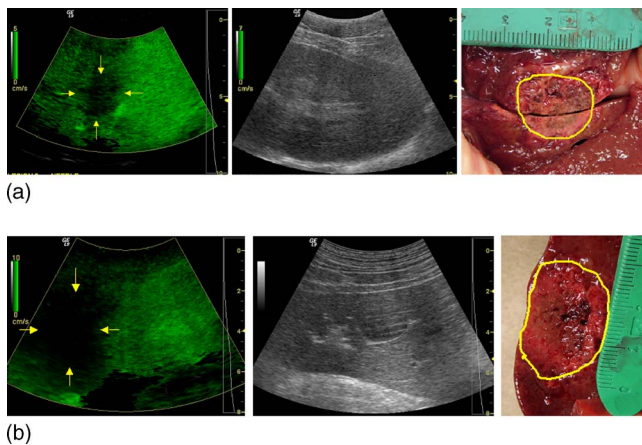
FIG. 12. Transabdominal sonoelastograms, coregistered sonograms, and gross pathology photographs of two hepatic RFA lesions. The lesion in (a) is located in two neighboring lobes as shown on the pathology photograph. The dimensions of this lesion are smaller in the sonoelastogram (19 mm × 17 mm) than in the gross pathology photograph (21 mm × 26 mm). The observers reported that the margin of the lesion in (b) was somewhat ambiguous in the sonoelastogram. In this case, the vibration was induced non-uniformly due to the difficulties in coupling of the vibration sources. Hence, a low signal to noise ratio is present on the left side of the sonoelastography image. Compared to the pathology findings (19 mm × 29 mm), the sonoelastography overestimates the size of the lesion (26 mm × 32 mm).

During our experiments, the respiratory motion was found to be a major source of artifacts. Since it was periodic, image acquisition was gated to obtain the 2D image of the lesion at the same phase of the respiratory cycle. This motion also affected the HIFU lesion generation and partially responsible for the irregular shape of lesions. Since the HIFU technique was used to create thermal lesions as a model for sonoelastography, the optimization of its therapeutic function is out of the scope of this article. However, in clinical practice, patient can hold their breath during the short period of HIFU exposure.

Some blood vessels within thermal treated region were not completely ablated by the HIFU approach due to flow-induced thermal dose reduction. The blood flow in these vessels was highlighted in sonoelastograms [Fig. 5(d)]. As a result, sonoelastography may also be helpful in identifying the extent of vascular destruction in the cancer treatment, and reduce the recurrence of cancer.

A typical *in vivo* RFA lesion consists of three concentric zones: the central pale necrotic zone, red rim, and outer pink rim. The central zone contains dead hepatocytes, the red rim contains hemorrhagic material and thrombosed vessels but no viable cells, and the outer pink rim is an admixture of hemorrhage and viable hepatocytes.[49] Similar findings were also shown for the HIFU lesions. Thus, it is plausible to take into account the red rim for accurately measuring lesion dimensions and area on a gross pathology photograph.

The appearance of bubble clouds can occur in both RFA and HIFU lesions and is a function of the local energy deposition. Even so the presence of gas bubbles did not interfere with sonoelastography for lesion boundary delineation, possibly due to the lack of predominant shadowing effect. This finding also indicates that gas bubbles may not notably change the stiffness of a thermal lesion. Interestingly, some of the HIFU lesions not present on B-mode were easily detected by sonoelastography. Thus, the HIFU lesion could be a good isoechoic model for the evaluation of ultrasound elastographic modalities.

V. CONCLUSIONS

In summary, 32 thermal lesions of various volumes ($0.2–5.3$ cm^3) were created and imaged by *in vivo* real-time sonoelastography. The area and volume of lesions measured by sonoelastography correlated closely to the pathology findings. This is in part attributed to the intrinsic stiffness contrast generated by the tissue ablation process. This study demonstrates that sonoelastography can be more reliable and accurate for *in vivo* imaging of hepatic thermal lesions in comparison to conventional ultrasound. For patients under-

going RFA or HIFU for liver cancer treatment, sonoelastography may potentially display treated lesion boundaries in real-time to assure adequate therapy. Future study will focus on the improvement of the quality of transabdominal sonoelastography by means of enhancing the transmission of mechanical vibration into the target organ.

ACKNOWLEDGEMENTS

a)Author to whom correspondence should be addressed. Telephone: 734-353-0388; Fax: 734-764-8541. Electronic mail: maggiez@umich.edu

[1] G. D. Dodd III, M. C. Soulen, R. A. Kane, T. Livraghi, W. R. Lees, Y. Yamashita, A. R. Gillams, O. I. Karahan, and H. Rhim, "Minimally invasive treatment of malignant hepatic tumors: at the threshold of a major breakthrough," Radiographics **20**, 9–27 (2000).

[2] L. Solbiati, T. Ierace, S. N. Goldberg, S. Sironi, T. Livraghi, R. Fiocca, G. Servadio, G. Rizzatto, P. R. Mueller, A. Del Maschio, and G. S. Gazelle, "Percutaneous US-guided radio-frequency tissue ablation of liver metastases: treatment and follow-up in 16 patients," Radiology **202**, 195–203 (1997).

[3] S. Rossi, M. Di Stasi, E. Buscarini, P. Quaretti, F. Garbagnati, L. Squassante, C. T. Paties, D. E. Silverman, and L. Buscarini, "Percutaneous RF interstitial thermal ablation in the treatment of hepatic cancer," AJR, Am. J. Roentgenol. **167**, 759–768 (1996).

[4] D. Choi, H. K. Lim, W. J. Lee, S. H. Kim, Y. H. Kim, S. H. Kim, and J. H. Lim, "Early assessment of the therapeutic response to radio frequency ablation for hepatocellular carcinoma: Utility of gray scale harmonic ultrasonography with a microbubble contrast agent," J. Ultrasound Med. **22**, 1163–1172 (2003).

[5] M. Morimoto, A. Nozawa, K. Numata, K. Shirato, K. Sugimori, A. Kokawa, N. Tomita, T. Saitou, Y. Nakatani, T. Imada, and K. Tanaka, "Evaluation using contrast-enhanced harmonic gray scale sonography after radio frequency ablation of small hepatocellular carcinoma: sonographic-histopathologic correlation," J. Ultrasound Med. **24**, 273–283 (2005).

[6] L. Solbiati, S. N. Goldberg, T. Ierace, M. Dellanoce, T. Livraghi, and G. S. Gazelle, "Radio-frequency ablation of hepatic metastases: postprocedural assessment with a US microbubble contrast agent-Early experience," Radiology **211**, 643–649 (1999).

[7] J. Hindley, W. M. Gedroyc, L. Regan, E. Stewart, C. Tempany, K. Hynnen, N. McDannold, Y. Inbar, Y. Itzchak, J. Rabinovici, H. S. Kim, J. F. Geschwind, G. Hesley, B. Gostout, T. Ehrenstein, S. Hengst, M. Sklair-Levy, A. Shushan, and F. Jolesz, "MRI guidance of focused ultrasound therapy of uterine fibroids: early results," AJR, Am. J. Roentgenol. **183**, 1713–1719 (2004).

[8] C. H. Cha, F. T. Lee, Jr., J. M. Gurney, B. K. Markhardt, T. F. Warner, F. Kelcz, and D. M. Mahvi, "CT versus sonography for monitoring radiofrequency ablation in a porcine liver," AJR, Am. J. Roentgenol. **175**, 705–711 (2000).

[9] T. A. Krouskop, D. R. Dougherty, and F. S. Vinson, "A pulsed Doppler ultrasonic system for making noninvasive measurements of the mechanical properties of soft tissue," J. Rehabil. Res. Dev. **24**, 1–8 (1987).

[10] R. M. Lerner, K. J. Parker, J. Holen, R. Gramiak, and R. C. Waag, "Sonoelasticity: Medical elasticity images derived from ultrasound signals in mechanically vibrated targets," Acoust. Imaging **16**, 317–327 (1988).

[11] K. J. Parker, S. R. Huang, R. A. Musulin, and R. M. Lerner, "Tissue response to mechanical vibrations for 'sonoelasticity imaging'," Ultrasound Med. Biol. **16**, 241–246 (1990).

[12] Y. Yamakoshi, J. Sato, and T. Sato, "Ultrasonic-imaging of internal vibration of soft-tissue under forced vibration," IEEE Trans. Ultrason. Ferroelectr. Freq. Control **37**, 45–53 (1990).

[13] J. Ophir, I. Cespedes, H. Ponnekanti, Y. Yazdi, and X. Li, "Elastography: A quantitative method for imaging the elasticity of biological tissues," Ultrason. Imaging **13**, 111–134 (1991).

[14] R. Righetti, F. Kallel, R. J. Stafford, R. E. Price, T. A. Krouskop, J. D. Hazle, and J. Ophir, "Elastographic characterization of HIFU-induced lesions in canine livers," Ultrasound Med. Biol. **25**, 1099–1113 (1999).

[15] T. Varghese, U. Techavipoo, W. Liu, J. A. Zagzebski, Q. Chen, G. Frank, and F. T. Lee, Jr., "Elastographic measurement of the area and volume of thermal lesions resulting from radiofrequency ablation: pathologic correlation," AJR, Am. J. Roentgenol. **181**, 701–707 (2003).

[16] S. Catheline, F. Wu, and M. Fink, "A solution to diffraction biases in sonoelasticity: the acoustic impulse technique," J. Acoust. Soc. Am. **105**, 2941–2950 (1999).

[17] L. Sandrin, M. Tanter, S. Catheline, and M. Fink, "Shear modulus imaging with 2-D transient elastography," IEEE Trans. Ultrason. Ferroelectr. Freq. Control **49**, 426–435 (2002).

[18] L. Sandrin, M. Tanter, J. L. Gennisson, S. Catheline, and M. Fink, "Shear elasticity probe for soft tissues with 1-D transient elastography," IEEE Trans. Ultrason. Ferroelectr. Freq. Control **49**, 436–446 (2002).

[19] J. Bercoff, M. Pernot, M. Tanter, and M. Fink, "Monitoring thermally-induced lesions with supersonic shear imaging," Ultrason. Imaging **26**, 71–84 (2004).

[20] J. Bercoff, M. Tanter, and M. Fink, "Supersonic shear imaging: a new technique for soft tissue elasticity mapping," IEEE Trans. Ultrason. Ferroelectr. Freq. Control **51**, 396–409 (2004).

[21] M. Fatemi and J. F. Greenleaf, "Ultrasound-stimulated vibro-acoustic spectrography," Science **280**, 82–85 (1998).

[22] K. R. Nightingale, M. L. Palmeri, R. W. Nightingale, and G. E. Trahey, "On the feasibility of remote palpation using acoustic radiation force," J. Acoust. Soc. Am. **110**, 625–634 (2001).

[23] K. R. Nightingale, M. S. Soo, R. W. Nightingale, and G. E. Trahey, "Acoustic radiation force impulse imaging: *in vivo* demonstration of clinical feasibility," Ultrasound Med. Biol. **28**, 227–235 (2002).

[24] A. P. Sarvazyan, O. V. Rudenko, S. D. Swanson, J. B. Fowlkes, and S. Y. Emelianov, "Shear wave elasticity imaging: a new ultrasonic technology of medical diagnostics," Ultrasound Med. Biol. **24**, 1419–1435 (1998).

[25] J. Bishop, G. Poole, M. Leitch, and D. B. Plewes, "Magnetic resonance imaging of shear wave propagation in excised tissue," J. Magn. Reson Imaging **8**, 1257–1265 (1998).

[26] J. B. Fowlkes, S. Y. Emelianov, J. G. Pipe, A. R. Skovoroda, P. L. Carson, R. S. Adler, and A. P. Sarvazyan, "Magnetic-resonance imaging techniques for detection of elasticity variation," Med. Phys. **22**, 1771–1778 (1995).

[27] R. Muthupillai, D. J. Lomas, P. J. Rossman, J. F. Greenleaf, A. Manduca, and R. L. Ehman, "Magnetic resonance elastography by direct visualization of propagating acoustic strain waves," Science **269**, 1854–1857 (1995).

[28] D. B. Plewes, I. Betty, S. N. Urchuk, and I. Soutar, "Visualizing tissue compliance with MR imaging," J. Magn. Reson Imaging **5**, 733–738 (1995).

[29] T. Wu, J. P. Felmlee, J. F. Greenleaf, S. J. Riederer, and R. L. Ehman, "Assessment of thermal tissue ablation with MR elastography," Magn. Reson. Med. **45**, 80–87 (2001).

[30] T. Varghese and H. Shi, "Elastographic imaging of thermal lesions in liver in-vivo using diaphragmatic stimuli," Ultrason. Imaging **26**, 18–28 (2004).

[31] T. Varghese, J. A. Zagzebski, and F. T. Lee, Jr., "Elastographic imaging of thermal lesions in the liver *in vivo* following radiofrequency ablation: preliminary results," Ultrasound Med. Biol. **28**, 1467–1473 (2002).

[32] B. J. Fahey, S. J. Hsu, P. D. Wolf, R. C. Nelson, and G. E. Trahey, "Liver ablation guidance with acoustic radiation force impulse imaging: challenges and opportunities," Phys. Med. Biol. **51**, 3785–3808 (2006).

[33] B. J. Fahey, K. R. Nightingale, S. A. McAleavey, M. L. Palmeri, P. D. Wolf, and G. E. Trahey, "Acoustic radiation force impulse imaging of myocardial radiofrequency ablation: Initial *in vivo* results," IEEE Trans. Ultrason. Ferroelectr. Freq. Control **52**, 631–641 (2005).

[34] R. Souchon, O. Rouviere, A. Gelet, V. Detti, S. Srinivasan, J. Ophir, and J. Y. Chapelon, "Visualisation of HIFU lesions using elastography of the human prostate *in vivo*: Preliminary results," Ultrasound Med. Biol. **29**, 1007–1015 (2003).

[35] L. Curiel, R. Souchon, O. Rouviere, A. Gelet, and J. Y. Chapelon, "Elastography for the follow-up of high-intensity focused ultrasound prostate cancer treatment: Initial comparison with MRI," Ultrasound Med. Biol.

31, 1461–1468 (2005).

[36]K. J. Parker, D. Fu, S. M. Graceswki, F. Yeung, and S. F. Levinson, "Vibration sonoelastography and the detectability of lesions," Ultrasound Med. Biol. **24**, 1437–1447 (1998).

[37]K. J. Parker and R. M. Lerner, "Sonoelasticity of organs: Shear waves ring a bell," J. Ultrasound Med. **11**, 387–392 (1992).

[38]L. S. Taylor, M. Zhang, J. G. Strang, D. J. Rubens, and K. J. Parker, "*In vitro* imaging of thermal lesions using three dimensional vibration sonoelastography," Proceedings of the Second International Symposium on Therapeutic Ultrasound, Seattle, Washington, 2002a, pp. 176–184 (unpublished).

[39]S. N. Goldberg, G. S. Gazelle, and P. R. Mueller, "Thermal ablation therapy for focal malignancy: A unified approach to underlying principles, techniques, and diagnostic imaging guidance," AJR, Am. J. Roentgenol. **174**, 323–331 (2000).

[40]L. S. Taylor, University of Rochester, 2002b.

[41]S. R. Huang, R. M. Lerner, and K. J. Parker, "On estimating the amplitude of harmonic vibration from the Doppler spectrum of reflected signals," J. Acoust. Soc. Am. **88**, 2702–2712 (1990).

[42]M. Zhang, B. Castaneda, Z. Wu, P. Nigwekar, J. V. Joseph, D. J. Rubens, and K. J. Parker, "Congruence of imaging estimators and mechanical measurements of viscoelastic properties of soft tissues," Ultrasound Med. Biol. **33**, 1617–1631 (2007).

[43]M. Zhang, P. Nigwekar, B. Castaneda, K. Hoyt, J. V. Joseph, A. di Sant'agnese, E. M. Messing, J. G. Strang, D. J. Rubens, and K. J. Parker, "Quantitative characterization of viscoelastic properties of human prostate correlated with histology," Ultrasound Med. Biol. **34**, 1033–1042 (2008).

[44]B. Castaneda, K. Hoyt, M. Zhang, D. Pasternack, L. Baxter, P. Nigwekar, A. di Sant'agnese, J. V. Joseph, J. G. Strang, D. J. Rubens, and K. J. Parker, "Prostate cancer detection based on three dimensional sonoelastography," Proceedings of the IEEE Ultrasonics Symposium, New York, New York, 2007, pp. 1353–1356 (unpublished).

[45]M. Z. Kiss, T. Varghese, and T. J. Hall, "Viscoelastic characterization of *in vitro* canine tissue," Phys. Med. Biol. **49**, 4207–4218 (2004).

[46]S. A. Kruse, J. A. Smith, A. J. Lawrence, M. A. Dresner, A. Manduca, J. F. Greenleaf, and R. L. Ehman, "Tissue characterization using magnetic resonance elastography: Preliminary results," Phys. Med. Biol. **45**, 1579–1590 (2000).

[47]Z. Liu and L. Bilston, "On the viscoelastic character of liver tissue: Experiments and modelling of the linear behaviour," Biorheology **37**, 191–201 (2000).

[48]G. Pareek, E. R. Wilkinson, S. Bharat, T. Varghese, P. F. Laeseke, F. T. Lee, Jr., T. F. Warner, J. A. Zagzebski, and S. Y. Nakada, "Elastographic measurements of *in-vivo* radiofrequency ablation lesions of the kidney," J. Endourol **20**, 959–964 (2006).

[49]S. S. Raman, D. S. Lu, D. J. Vodopich, J. Sayre, and C. Lassman, "Creation of radiofrequency lesions in a porcine model: Correlation with sonography, CT, and histopathology," AJR, Am. J. Roentgenol. **175**, 1253–1258 (2000).